Chapter

In Situ TEM Studies of III-V Nanowire Growth Mechanism

Carina B. Maliakkal

Abstract

Growing nanowires inside a transmission electron microscope (TEM) and observing the process in situ has contributed immensely to understanding nanowire growth mechanisms. Majority of such studies were on elemental semiconductors – either Si or Ge – both of which are indirect bandgap semiconductors. Several compound semiconductors on the other hand have a direct bandgap making them more efficient in several applications involving light absorption or emission. During compound nanowire growth using a metal catalyst, the difference in miscibility of the nanowire species inside the metal catalyst are different, making its growth dynamics different from elemental nanowires. Thus, studies specifically focusing on compound nanowires are necessary for understanding its growth dynamics. This chapter reviews the recent progresses in the understanding of compound semiconductor nanowire growth obtained using in situ TEM. The concentrations of the nanowire species in the catalyst was studied in situ. This concentration difference has been shown to enable independent control of layer nucleation and layer growth in nanowires. In situ TEM has also enabled better understanding of the formation of metastable crystal structures in nanowires.

Keywords: compound nanowire, transmission electron microscopy, ledge-flow, semiconductor, GaAs, in situ techniques, wurtzite, zincblende, polytypism

1. Introduction

The high surface-to-volume ratio and the high aspect ratio of the nanowire geometry paves the way to a plethora of interesting advantages. Growing materials as nanowires has enabled the formation of metastable crystal phases, in turn enabling crystal structure tuning [1–4]. Integration of different lattice-mismatched materials into the same structure was also achieved; compared to growth of heteroepitaxial films, defect-free growth is easier in nanowires because of the small diameter (a few 10 or 100 nanometers) and small interfacial area [5–7]. Yet another advantage of nanowire growth is to form alloy compositions which are unstable in the bulk phase [8]. Materials generally grown in the nanowire morphology can be broadly classified as elemental and compound [9]. Metallic nanowires (Ti, Fe, Co, Ni, Sn etc.) and elemental semiconductors (e.g. Si, Ge) fall under the category of elemental materials. Stochiometric compound nanowires are either compound semiconductors (e.g. GaAs, ZnO) or insulators (e.g. Al_2O_3, Si_3N_4). Alloy nanowires are also possible, e.g. Si_xGe_{1-x}, $Al_xGa_{1-x}As$. Controlling the electronic, bandgap-engineering related, structural, compositional, morphological, mechanical and optical properties of semiconductor nanowires enables its application in devices such

solar cells, [10–13] electronics, [14–16] LEDs, [16, 17] LASERS, [18, 19] photodetectors, [20, 21] thermoelectrics, [22, 23] biosensors [24, 25] and qubits [26–29].

Nanowires can be fabricated by a top-down approach (where regions of a film are selectively etched) or by a bottom-up approach (where the nanowires are grown on a substrate) [30]. Top-down approach often result in rough defected surfaces [9]. One way to grow nanowires bottom-up is by electrochemical deposition [31–34]. The bottom-up growth of nanowires from a gas phase precursor supply is what we will discuss in more detail here. The bottom-up nanowires growth from gas phase are done either with or without a foreign metal catalyst. The nanowire growth using a metal catalyst was proposed to proceed by the vapor–liquid–solid or 'VLS' mechanism [35]. According to the VLS mechanism, the nanowire elements or their precursor supplied in the vapor (V) phase gets dissolved in the liquid (L) 'catalyst' and after supersaturation precipitates out as the solid (S) nanowire (**Figure 1**). The metallic liquid, in addition to providing a nucleation point for the solid nanowire, fosters the gathering and in some cases the decomposition of precursors – hence often called 'catalyst' [9]. Later a similar growth mode called the vapor-solid–solid (VSS) was also proposed for when the catalyst is a solid, instead of the liquid catalyst in VLS [36, 37]. When there is no foreign catalyst used the nanowire growth can proceed in either of the two ways: (i) a self-catalyzed mode where the metallic element of the nanowire forms the liquid catalyst droplet [38–40] or (ii) a non-catalyzed vapor-solid route where the material from the vapor phase directly attaches to the solid nanowire without any liquid or solid catalyst [41]. The yield of nanowire growth without an external catalyst can be increased by the use of selective-area dielectric mask to keep some areas unfavorable for nucleation; small openings in the mask acting as preferential nucleation site for nanowires [42, 43].

Some of the common techniques for growing nanowires with gas phase precursors by the aforementioned mechanisms include chemical vapor deposition (CVD), metalorganic CVD (MOCVD) and molecular beam epitaxy (MBE). These systems were initially designed for growing thin films and later adapted for growing nanowires. Usually for growing nanowires in any of these systems the catalyst-coated substrate is loaded into the system, the system is closed and precursors are supplied at

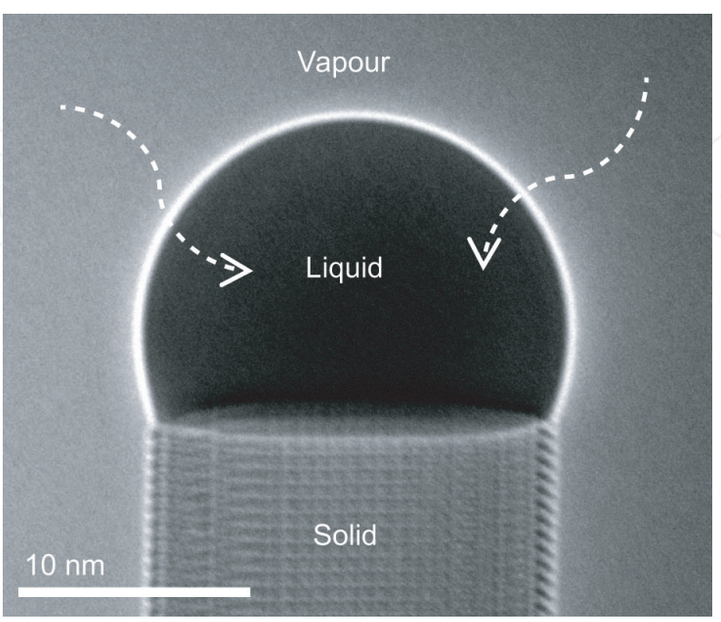

Figure 1.
Nanowire growth with a liquid catalyst is explained by the VLS mechanism. Accordingly, the supplied vapor phase precursor species dissolves in the liquid catalyst and at appropriately high supersaturation crystallizes atomic layers of the solid nanowire. The TEM image shown here was captured in situ while an atomic layer was growing.

appropriate temperature and pressure. In conventional growth systems, either there is no in situ monitoring during growth or there is some large-area indirect monitoring. MBE systems sometimes monitors the crystal structure of the surface layer by RHEED (reflection high-energy electron diffraction). Some MOCVD systems are equipped with in situ light reflectance monitors which can be used to estimate the increase in sample height and surface roughening. These methods are used conventionally for tracking growth of thin films from large areas of the sample. Using these techniques for monitoring nanowires demand some modifications. After growing nanowires, the samples can be elaborately analyzed ex situ by methods relevant to the study. Typical characterization techniques are scanning electron microscopy (SEM), transmission electron microscopy (TEM), X-ray diffraction (XRD), energy dispersive X-ray spectroscopy (XEDS), photoluminescence, etc.

Such ex situ characterizations could suffice for studying nanowire morphology, crystallinity and composition. Analysis of nanowires from multiple growths with different parameters can help indirectly understand the growth mechanism to some extent. Still the dynamics of the growth understood based on such ex situ characterizations are largely speculative. Moreover, some attributes of the nanowire could be different while growing (at high temperature with precursor supply) and after cooling down the system for post mortem analysis. Monitoring nanowire growth in situ certainly has advantages in elucidating the growth mechanism and dynamics. An example of a phenomenon which was discovered only due to in situ observation of individual nanowires is truncation — where the nanowire-catalyst interface has a dynamic non-flat surface near the triple-phase-line [44–48]. (Triple-phase-line refers to the periphery of the interface between the nanowire and the catalyst droplet where the vapor, liquid and solid phases meet.) Another interesting in situ observation was that the nucleation of wurtzite layer happens at, or at least very close to, a corner of the triple-phase-line (observation of the precise location being elusive due to the 'limited' temporal resolution compared to the expected extremely rapid growth of the nucleus to beyond the critical size) [49].

2. In situ techniques

Observing and characterizing the nanowires while they are growing is called in situ growth monitoring. Strictly speaking, 'in operando' is the exact word, but we stick to 'in situ' to conform to popular usage. In situ techniques can provide directly interpretable and time-resolved observations enabling better understanding of the growth mechanism, which in turn empowers better control of nanowire growth for specific technological applications.

In situ characterization of nanowire crystal structure or nanowire morphology has been reported using various techniques. In situ RHEED attached to MBE systems can be used to follow crystal structure changes and nucleation/birth of ensemble of nanowires [50, 51]. By modifying the optical reflectometry techniques that have been used conventionally in MOCVD systems, the nanowire diameter and length evolution has been monitored in situ in real time for an ordered array of nanowires [52]. Combining finite difference frequency domain simulations with in situ reflectometry enabled monitoring growth of randomly positioned nanowires (i.e. periodic array was not a necessity) [53]. In situ X-ray diffraction (XRD) has been used to study crystal phase of the nanowire [54, 55] and the catalyst phase [56]. In situ infrared spectroscopy has been used to correlate surface chemistry during nanowire growth to its morphology [57–59] or the choice of growth direction [60]. Line-of-sight quadrupole mass spectrometry in situ was used to study different stages of nanowire growth including nanowire nucleation [61]. All these techniques give ensemble averaged results.

In situ imaging techniques on the other hand allows monitoring individual nanowires. Optical microscopes due to the limited spatial resolution are not ideal for observing growth evolution of nanowire (though some studies have been attempted using confocal optical microscopy using photoluminescence measurements [62]). Scanning electron microscopes (SEMs) have better spatial resolution than optical microscopes and could be used to monitor nanowire growth [63–67]. In situ SEM combined with Auger electron spectroscopy has been used to correlate nanowire growth and morphology to surface chemistry [63]. In situ electron backscattered electron diffraction (EBSD) performed during growth in an SEM has been used to study crystal phases and crystallographic orientation [64]. An SEM uses electron scattering from a sample while a transmission electron microscope (TEM) uses the electrons transmitted through a thin sample (preferably less than ~50 nm) to form images. TEMs have better spatial resolution than SEMs. Be it in an in situ SEM or TEM study, a video or a series of images are captured to study the dynamics of the process in relation with the specimen environment. A key advantage of using in situ microscopic techniques, particularly in situ TEM, is that localized or dynamic behavior happening at individual wires could be investigated. One limitation to studying nanowire growth inside a microscope is that electron microscopes require vacuum environment to minimize electron scattering in the air outside the specimen. So, often the growth conditions, e.g. pressure, used for the in situ growth study are slightly modified compared to a conventional growth method. Typical total pressures used in conventional ex situ CVD are much beyond the maximum attainable pressure for in situ TEM experiments. Majority of the pressure in the ex situ CVD case is from the carrier gas. By careful design of the TEM and the growth chamber, it is in principle possible to obtain comparable precursor partial pressures.

3. Techniques for growth nanowire by in situ TEM

The very first demonstration of nanowire growth by in situ TEM was from Prof. Yang's group which validated the VLS mechanism experimentally using the Au-catalyzed Ge nanowire growth [68]. This seminal experiment was conducted by heating Au nanoclusters along with micrometer-sized Ge particles. They neither used a continuous supply of Ge-precursor nor a closed system. Over the course of time technological advances in the field of TEM paved the way to environmental TEM (ETEM), where the pressure near the sample can be orders of magnitude higher than a conventional TEM. Studies in which a continuous supply of precursors was used were reported [41, 46–49, 69–90].

However, an ETEM is not a necessity for studying CVD nanowire growth in situ by TEM, it is possible by using a closed or isolated cell instead. In principle, it is possible that a cell isolated from the microscope vacuum is used; gaseous precursors can be supplied continuously to this cell by external inlet gas-tubes and removed by outlet tubes, without releasing the gases to the microscope environment. Another strategy is to use completely closed cells, in which powders of precursor material are deposited in the cell and then sealed [91]. These powders are heated intentionally to evaporate it so as to form a vapor-phase supply of precursors to the catalyst for growth [91]. An intermediate method, which is feasible with commercially available instruments for gas handling, is to pre-deposit powdered material on the isolated cell but externally supply carrier gases such as H_2 or N_2 (no gases are released here to the microscope environment) [92]. The cells have an electron transparent amorphous film both at the top and at the bottom of the cell. An advantage of this strategy is that any ordinary TEM can be used for it. However, the thickness of the top and bottom casing combined could be substantial, reducing the attainable spatial resolution.

In the more conventional open heating cell geometry, there is either one layer of amorphous layer or none, providing better spatial resolution. Commercial chips are available with a few holes made in a thin amorphous film. When a piece of commercially available substrate wafer is loaded vertically in the TEM [69, 70] or a lithographically patterned cantilever chips is used [76, 93] for growing epitaxial aligned nanowires there is no film on top or bottom of the nanowire sample, enabling epitaxial growth and better spatial resolution; in such cases the resolution of the microscope and thickness of the sample would be the bottleneck. TEM resolution is currently restricted by technical limitations, not by the physically attainable limit; over the years TEM resolution has been constantly improving and this evolution is visible if we look at reports of nanowire growth with in situ TEM as well.

4. In situ TEM of elemental semiconductor nanowire growth

Si and Ge nanowire growth has been extensively studied by in situ TEM [46, 68–78, 81, 82, 85–88]. Several aspects such as diameter dependance of growth kinetics [70], nucleation kinetics [87], surface faceting [69], surface migration of catalyst (Au) on nanowire (Si) surface [71], tapering [94], and kinking [75] have been investigated. Depending on the growth conditions such as temperature, catalyst particle and precursor pressures the growth proceeds either by the VLS mode [46, 68–72, 74–76, 78, 81, 82, 85–88] or the VSS mode [46, 72–74, 77, 78, 82, 88]. It is interesting to note that VLS growth has been observed to occur even below the eutectic temperature [72].

The nanowire catalyst interface is atomically flat, except when a ledge is growing. The layer-by-layer growth of nanowire atomic layers has been studied in situ during the VLS growth of elemental nanowires [74, 78]. A new (bi)layer starts only after the previous one is completely grown (at least for the nanowire diameters studied) [74, 78]. The time each layer takes to complete once it has nucleated can be called ledge-flow time (or layer completion time, also called step-flow time in some references). We will use the term incubation time for the difference between the ending of one layer and the start of the next layer. (This is not to be confused with the incubation time before the birth/nucleation of the nanowire itself). In VLS growth of elemental nanowires each layer grows instantaneously (ledge-flow time ~ 0) while there is a significant incubation/waiting time between successive layer-growth events [74, 78]. This observation can be explained by a very simple argument — the amount of material required to raise the chemical potential high enough to nucleate a layer is sufficient for forming one full layer as soon as it nucleates. So the layer grows rapidly once nucleated [74]. There is a considerable incubation time, which in turn determines the average nanowire growth rate.

Most theoretical models for nanowire growth kinetics assume instantaneous layer completion and the growth rate is calculated in a nucleation-limited regime [95–98]. This assumption seems to be valid for the VLS growth of elemental nanowires we discussed above. However, we will now discuss in this section about elemental nanowires and the next section about compound nanowires cases where this assumption of instantaneous layer-growth breaks down.

As mentioned before, the growth can proceed by the VSS route where the catalyst is a solid particle. In the VSS growth of elemental nanowires the layer completion is slow [73, 74, 78, 82]. The incubation time in the VSS case is shorter than in VLS [74, 78]. The solubility of the growth material in the solid catalyst is much lower than in a liquid catalyst, thus a small amount of excess species can increase the chemical potential sufficiently to nucleate a new layer — making the incubation time short [74, 78]. But the limited amount of material present could be insufficient

for forming a complete bilayer, in turn making the ledge-flow process slow [74, 78]. The limited solubility of the nanowire species inside the solid catalyst offers the opportunity to grow compositionally abrupt axial heterostructure [74]. Another interesting aspect about VSS growth of elemental nanowires is that there can be two or more ledges growing simultaneously [73, 78, 82]. This also is in contrast to VLS growth of elemental nanowires were a second ledge starts only after the first is fully grown.

5. In situ compound nanowire growth

Compound nanowires grown inside TEM include insulator materials (Al_2O_3 [45]) and semiconductors (GaAs [49, 84, 99], GaN [79, 83, 100], GaP [46, 80], InAs [91] and PdSe [92]). VSS growth of compound nanowires in a TEM with a supply of precursors has not been reported so far; hence the discussion we have in this section is restricted to VLS growth of compound nanowires. In the cases where atomic resolution videos where obtained, ledge-flow was not instantaneous [49, 83, 84, 90]. The initial studies of MOCVD combined with in situ TEM were at very low precursor pressures compared to the typical 'ex situ' MOCVD; [83, 84] hence it was not sure if the gradual ledge-flow was representative of ex situ growths as well. The latest report was with orders of magnitude higher pressures than previous studies, but still the precursor pressures values were on the lower end of conventional ex situ MOCVD growth parameter regime [90]. If or not the ledge-flow of atomic layers is gradual in the entire range of growth parameters used in ex situ growths is yet to be investigated.

The gradual ledge-flow growth in compound nanowires, is in striking contrast to the VLS monoatomic nanowire growth. But this difference between elemental and compound nanowires is simple to understand. In elemental nanowire only one material species controls both nucleation and layer-growth events. For example, during Si nanowire growth with a Au catalyst the Si dissolving in the Au is the key factor. At typical growth temperatures of Si nanowire growth (400–600°C) the liquidus line where the Au-Si system is at equilibrium is with about 20–28% Si (depending on the growth temperature). A little extra Si is insufficient to supersaturate the system enough to trigger a nucleation event. The amount of excess Si that accumulates during the incubation time and triggers the nucleation of a layer could thus suffice to form an entire layer. However, in a compound nanowire case the miscibility of two different nanowire species within the catalyst could be decisive, in turn making the dynamics more complex. Species like Ga, In, Al and Zn alloys readily with Au while species like As, N, P and O are hardly soluble in Au [101]. In the case of Au-catalyzed GaAs growth, for example, theoretical calculations predicted that Ga mixes readily in Au but As has poor solubility in Au [102, 103]. Experimental studies of the catalyst composition was mostly done ex situ post growth until very recently.

6. Catalyst composition measured in situ

Understanding the concentration of the different species during growth is key to understanding the growth dynamics. Parameters like surface and interface energies, vapor pressure and chemical potential of the catalyst are dependent on the catalyst composition [104–106]. The catalyst composition measured ex situ depends not just on the growth parameters, but also on the conditions used to terminate growth and cool down the sample (the ambient gas, ramp down rate etc.) [2, 44, 107]. Typically

in MOCVD the temperature is decreased from the growth temperature down to either room temperature or an intermediate temperature in a group V (or group VI) precursor environment to prevent etching and surface roughening. At the initial part of this ramp down, where the temperature is still adequate to grow, the group III (or II) species already present in the catalyst reacts with the group V precursor to form an additional nanowire segment, in turn decreasing the concentration of the group III species in the catalyst [2, 44, 107]. Hence in situ measurement is key.

Recently in situ measurement of the catalyst composition during the growth process was reported [89]. X-ray energy dispersive spectroscopy (XEDS) spectroscopy was used in situ to study the catalyst composition during Au-catalyzed GaAs growth performed inside an ETEM. Trimethylgallium (TMGa) and arsine (AsH_3) were used as the precursors. The XEDS measurement was conducted in the TEM mode by condensing the beam to a small region and positioning it in the front part of the catalyst (like depicted in **Figure 2a**). Since the nanowire was growing, the sample stage was constantly repositioned so that the beam is all the time on the catalyst itself, and not hitting the nanowire part. The XEDS signal from Au, Ga and As was studied. The catalyst had a significant amount of Ga alloyed with the Au. The Ga % in the catalyst was found to increase with both temperature and the Ga precursor flux. **Figure 2b** shows the Ga % as function of the V/III ratio i.e. the ratio of the group V precursor to the group III precursor. These experiments were done in the 420–500°C temperature range. At these temperatures, the catalyst interaction with nanowire depends on the TMGa flow – (a) in the absence of a TMGa flow the catalyst particle can etch the nanowire (similar to what was reported by Tornberg *et al*. [108]); (b) at an intermediate TMGa flow there is neither growth nor etching; (c) at a slightly higher TMGa there is nanowire growth where the Ga % increases with increasing TMGa flow to a quasi-steady state and the catalyst bulges due to the additional Ga; (d) eventually there is a regime with truncated nanowire-catalyst interface and (e) finally at even higher TMGa the catalyst bulges and topples.

The As signal in the EDX spectra was too low to be conclusively attributed to be arising from the catalyst and was suspected to be due to scattered signal from the nanowire [89]. The As content was however estimated by an indirect method — calculating phase diagrams or liquidus lines for different As % and comparing the Ga % in these calculations to the measured Ga % value. The estimated minimum As % in the catalyst was ~0.01%. For the nanowire dimensions used, this would be

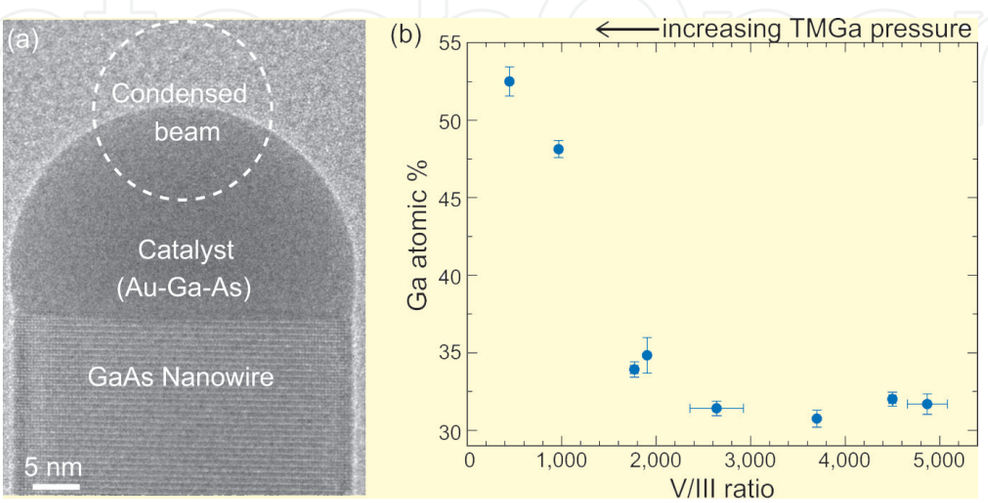

Figure 2.
In situ catalyst composition measurement. (a) TEM image of a nanowire. The catalyst composition was measured in situ by XEDS by condensing the beam in the front of the catalyst. (b) the Ga % in the catalyst is plotted as a function of the V/III ratio. The As % measured in the catalyst was negligible. (a) and (b) are adapted from Maliakkal et al. *2019 [89] with permission as per creative commons license.*

less than the amount of As required to form one complete bilayer. Indirect estimates based on ex situ growth, [95] phase diagrams, [109] and theoretical calculations related to Au-catalyzed GaAs nanowire growth [102, 103] also suggested low As solubility in the Au-Ga alloy.

7. Independent control of layer nucleation and layer-growth

The concentration difference between the two different nanowire species in the catalyst [89] implies that both these species could affect the growth in different ways. This was studied in detail, again using Au-catalyzed GaAs (and TMGa and AsH_3 as precursors) [90]. Two sets of experiments were investigated – one was a TMGa series (where AsH_3 and temperature were kept constant) and a second was AsH_3 series (where TMGa and temperature were kept constant). The ledge-flow time was found to decrease drastically with increasing AsH_3 flow (**Figure 3b**); thus the ledge-flow process was understood to be limited by the As availability. This agrees well with the low As % present in the catalyst [89]. (The idea that ledge-flow is limited by As availability was proposed in an earlier study [84] but not elaborately investigated there.) On increasing TMGa flow in a separate experiment the incubation time decreased drastically while the ledge-flow time remained rather unchanged (**Figure 3c**). This indicated that nucleation of a new layer is triggered by excess Ga.

The experimental observations for the TMGa and AsH_3 series matched stochastic Monte Carlo simulations done based on mass transport and nucleation theory [89]. An example of how As % and Ga % in the catalyst varies in an almost cyclic way during the simulated layer-growth cycle is shown in **Figure 3d**.

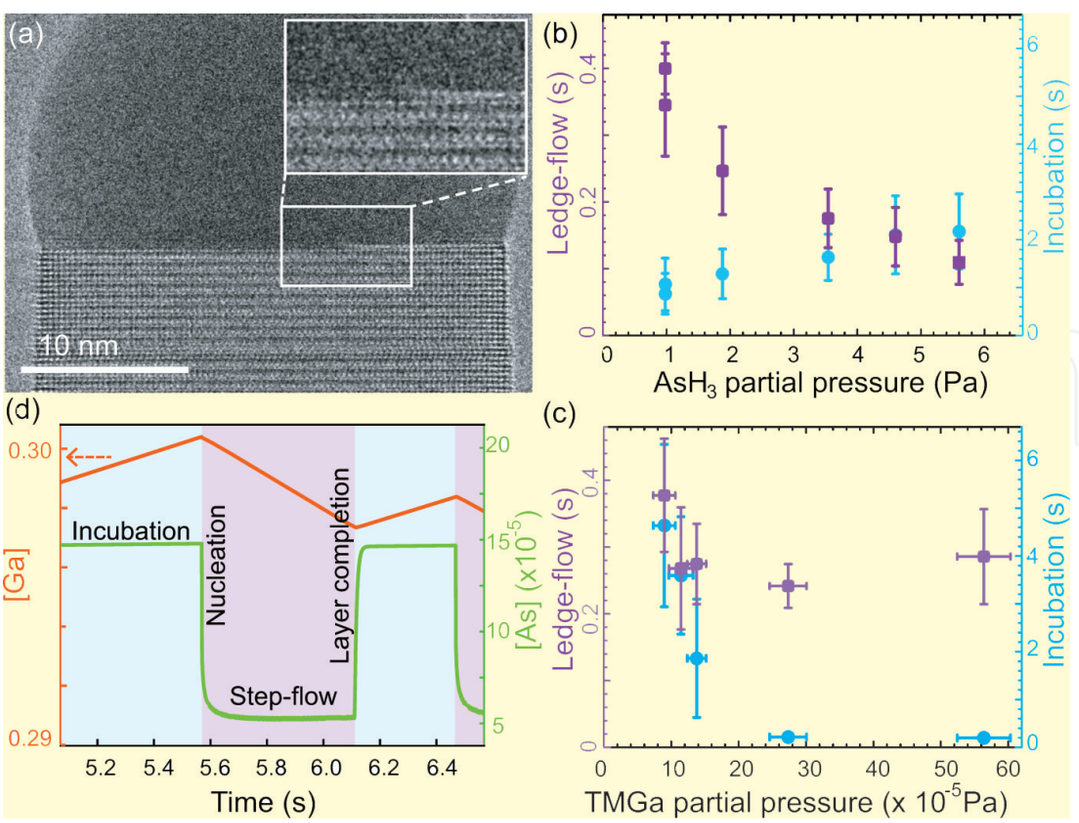

Figure 3.
(a) TEM image showing ledge-flow growth of an atomic bilayer. (b,c) Ledge-flow time as a function of As-precursor flow (b) and Ga-precursor flow (c). (d) A representative example of simulation of Ga and As concentrations in the catalyst. (Plots (b), (c) and (d) are adapted from Maliakkal et al. *[90] with permission. Further permissions should be directed to ACS.)*

During the incubation process the As concentration in the catalyst is in equilibrium with the ambient vapor. Once the layer nucleation happens the 'excess' As is consumed to form the GaAs nucleus and so As concentration quickly drops to a low level (where the As is in equilibrium with the solid GaAs nanowire). As soon as the layer is grown completely, the As % quickly rises and equilibrates again with the ambient vapor. Once this happens, the As contribution to the liquid supersaturation remains the same over the rest of the incubation period. However, the Ga building up in the catalyst keeps increasing the liquid chemical potential. Eventually, at some point after the liquid chemical potential is higher than the nucleation barrier, stochastically a nucleation event happens. Since the As % remains steady during the latter part of the incubation period, it is the Ga which is triggering nucleation of a new layer [90].

The study demonstrated independent control of layer nucleation (by Ga) and layer completion (by As) in GaAs nanowires growth [90]. The underlying reason for the nucleation of layer and ledge-flow to be controllable independently is the very low solubility of As and the high solubility of Ga in the Au catalyst. Several other III-V and II-VI compound semiconductors also consist of a nonmetallic species (group V or VI, e.g., N, O, P, S), and a metallic species (group II or III, e.g., Ga, In, Zn, Mg) [101]. These nonmetallic species typically dissolve very little in catalyst (gold or other typical transition metal catalysts) while the metallic species readily forms alloys. In cases were the amount of nonmetallic species collected in the catalyst and available for growth is low, the layer growth process will be restricted by availability of this nonmetallic species. Thus, independent control of layer nucleation and growth would be possible in several other nanowire systems too [90].

The occasions where controlling the layer nucleation and growth are extremely relevant could include doping and growth of ternary compounds. In VLS growth, the nucleation stage determines the crystal stacking of the entire atomic layer [1]. However, dopant/impurity incorporation happening would strongly depend on ledge-flow. Since impurity incorporation could be happening due to step trapping, a slow ledge-flow would help limit the impurity incorporation. On the contrary, for higher dopant incorporation, a fast ledge-flow could be advantageous [90].

8. Polytypism in III-V nanowires

Layer nucleation and growth for the different polytypes have been studied by in situ TEM. Before we discuss the key in situ results, let us discuss the concept of polytypism in nanowires and how the metastable structure could form. Nanowires enable the formation of metastable crystalline phases which do not form during its bulk growth. For example, most III-arsenides and III-phosphides form in the zincblende polytype when grown in bulk, because the bulk energy is lower for zincblende than wurtzite phase. But these materials can form in the wurtzite polytype in nanowires due to surface effects [2–4, 44, 110]. (Details of these crystal structures can be found elsewhere [4]). Controlled polytypism has great technological relevance because the electronic band structure depends on crystal structure. For example, GaP in the usual zincblende phase is an indirect bandgap material; while the wurtzite polytype has a pseudo-direct bandgap [111–113]. The valence and conduction bands of the two polytypes are often misaligned, so sections of one polytype in a matrix of the other polytype nanowire can confine electrons and/or holes. This enables crystal phase quantum dots with abrupt interfaces [114, 115]. Compositional quantum dots, on the other hand, often has a gradual variation of the composition (depending on the material combination chosen) deteriorating its properties.

Now let us first briefly discuss a simplified explanation for the occurrence of the metastable wurtzite structure in nanowires. During VLS growth, at appropriate catalyst contact angles, the nucleus of each layer is preferably formed at the triple-phase-line because it eliminates the energy cost of a preexisting liquid segment [1]. For nucleation happening at the triple-phase-line the nanowire surface energy is a key factor [1]. The surface energy of possible wurtzite side facets could be lower than the zincblende counterparts [1]. In such cases, the wurtzite structure can be more favorable than zincblende for energy minimization, depending on the catalyst supersaturation and relevant interface energies [1]. Extensive models proposed by several groups to correlate the observed crystal structure at different conditions can be found elsewhere [1, 96, 103, 104, 116–118].

In GaAs nanowire growth studied ex situ for a very wide range of V/III ratios it was found that very low V/III ratios gives zincblende, a higher V/III results in wurtzite, and an even higher V/III give zincblende again [110]. A high V/III ratio (i.e. higher AsH_3, which may also be interpreted as effectively lesser Ga) is associated with a smaller catalyst; while a low V/III results in bulged up catalyst with high contact angle [110]. There are also two intermediate transition regimes with mixed structures [110]. Theoretical models of Au-catalyzed GaAs growths could also simulate three different growth regimes [103, 104]. Often in typical experiment series a narrower range of V/III is studied, and thus it may happen that only a zincblende to wurtzite transition or only a wurtzite to zincblende transition is observed on increasing V/III ratio.

Jacobsson *et al.* observed two growth regimes in situ — at moderate V/III ratio wurtzite segments grew, and at low V/III the catalyst bulges and zincblende segments grew [84]. The wurtzite growth occurred while the nanowire-catalyst interface was one flat plane and the ledge-flow growth was gradual [84]. During zincblende growth the interface showed an oscillating truncated corner; the ledge-flow was "too rapid to observe" but was correlated to the cyclic dynamics of the truncation [84]. According to the study zincblende phase grows if any edge is truncated, whereas wurtzite grows only when the interface is flat [84]. They speculated that the truncation happening in the low V/III regime would make nucleation occur away from the triple-phase-line which in turn makes zincblende the preferred structure. (Note the authors had not claimed an if-and-only-if condition between interface geometry and crystal structure. However, in my personal experience, some readers misinterpreted that truncation was a necessity for low V/III zincblende growth.) The droplet contact angle was the key parameter in deciding the crystal structure [84]. Au:Ga ratio in the droplet was found to be not critical, hence a similar crystal structure–geometry correlation was speculated to be applicable to self-catalyzed wires too [84].

Polytypism in self-catalyzed GaAs nanowires was recently studied using in situ TEM-MBE by Panciera *et al* [99]. In this work the three regimes were observed as shown in **Figure 4e**, **g** and **h** (zincblende at low V/III ratio, wurtzite at higher V/III ratio, zincblende at even higher V/III ratio) [99]. In the high V/III zincblende regime, (which was not experimentally achievable in Jacobsson *et al.*), the nucleation was found to occur at the triple-phase-line, the ledge-flow was slow, and no truncation was observed. Their observations consistent with Jacobsson *et al.* include (i) control of crystal structure by contact angle, (ii) gradual ledge-flow and flat interface during wurtzite growth, and (iii) truncation and rapid ledge-flow observed in the low V/III zincblende growth [99].

However, it is not necessary that the low V/III zincblende growth can occur only with truncation. The growth of zincblende with a bulged particle (high contact angle) at low V/III ratio, but without truncation, has also been reported (**Figure 4f**) [89]. In this study the V/III ratio was decreased to observe bulging of the particle,

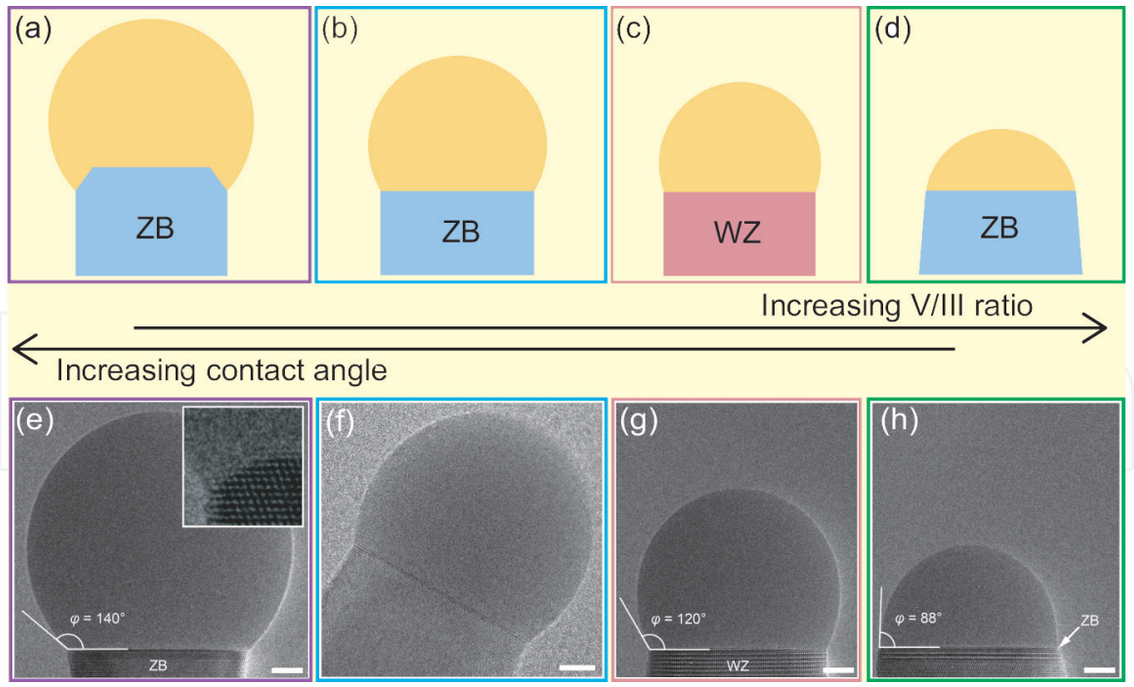

Figure 4.
(a)-(d) Schematic representation of crystal phases observed as a function of V/III ratio or catalyst contact angle. The catalyst-nanowire interface is either a single plane (b-d) or truncated (a). (e)-(h) shows TEM images with zincblende (ZB) or wurtzite (WZ) structures. Scalebars correspond to 5 nm. Inset of (e) shows a dynamic truncated corner during the zincblende growth at low V/III ratio. (e), (g) and (h) are adapted with permission from Panciera et al. *[99] Copyright (2020) American Chemical Society. Image (f) showing low V/III zincblende growth even without truncation is from another study – Maliakkal et al. [89]. Adapted with permission as per Creative Commons license.*

but a lower limit was set on the V/III ratio intentionally to avoid the truncation regime [89]. The V/III ratio was varied in small steps and maintained for some time to reach steady state [89] – this could be the reason why this intermediate zincblende regime with high contact angle and without truncation was observed in this study unlike the other two in situ studies discussed above [84, 99]. Thus, we can infer that the zincblende growth at low V/III does not necessarily require truncation. More detailed investigation is necessary to say if the nucleation happened at the triple-phase-line or the center in this case, and if the ledge-flow was gradual or instantaneous. Whether the presence of truncation makes the nucleation preferable away from the triple phase line is also an open question.

A heuristic explanation for the choice of crystal structure based on the currently available data [84, 89, 99] and theoretical calculations [1, 49] on GaAs VLS growth is as follows. The metastable wurtzite phase can grow only if the layer nucleates at the triple-phase-line [49]. If the nucleation is at triple-phase-line, either wurtzite or zincblende can form depending on the supersaturation and surface energies [1]. When nucleation occurs away from the triple-phase-line, it can form only zincblende structure [1, 49]. Now let us look at crystal structure as a function of the contact angle. Glas *et al.* predicted that nucleation is preferred at the triple-phase-line for a range of contact angles $[\pi - \beta_c; \beta_c]$, where the critical angle β_c is a function of the relevant interface energies [1, 49]. Thus, at intermediate contact angles (i.e. intermediate V/III ratios), nucleation occurs at the triple-phase-line and wurtzite structure is formed as observed(**Figure 4c**,**g**) [99]. For the lower contact angle (**Figure 4d**,**h**), nucleation was reported to be zincblende and at the triple-phase-line, [99] which demands that zincblende structure would have been the lower energy nucleus phase at those growth conditions [1]. For the higher contact angle regime, zincblende was found to grow, even without truncation [89]. It would have happened either (i) with nucleation away from the triple-phase-line giving

zincblende structure or (ii) with nucleation at the triple-phase-line only, but with the zincblende structure having lower energy at those growth conditions. Note that in the above explanation or in references [1, 49] truncation was not explicitly needed to explain crystal phase switching. At extremely high contact angles and at extremely low contact angles, there could be either truncation or large tapering; [84, 99] but truncation is not a necessity for zincblende growth. The truncation might be responsible for the observed quasi-instantaneous ledge-flow though.

9. Open questions

Ideally, for an exact explanation of nanowire crystal phases at different conditions discussed above, one could theoretically model the system and compare the contact angles where the structure is predicted to switch phases and compare it with experimental values. Such calculations, and also models for other phenomena in nanowires, involve different interface energy terms. However, there are hardly any direct experimental measurements of interface energies at the different growth conditions even for common material systems. The solid surface energies (the solid-vapor interface energy to be more precise) would depend on the surface relaxations/reconstructions adapted by the system, which again depends on the growth condition [119]. There exists post-growth surface energy measurements on bulk materials, [120] but is inadequate for knowing nanowire surface energies during growth conditions. Some roundabout estimates have been made by comparing experimental observations with approximate models for finding surface energies during growth; [99, 108] having these values are certainly better than having nothing, but we need better measurements. The reason for not having more direct measurements is simple – they are challenging to perform and observe at nanowire growth conditions. The surface tension of Au-Si liquid catalyst has been beautifully measured by studying electric field-induced deformation [85]. This method can be used to study other material systems as well. We have to come up with smart strategies for measuring solid–liquid and solid-vapor interface energies.

A seemingly basic, but still ambiguous topic is what are the key parameters deciding the nanowire growth direction. For example, unless at very peculiar growth conditions, most III-V and II-VI nanowires grow in the <111>/<0001> B direction, [3, 4] even on amorphous substrates, [89, 113, 121] in fact even without a substrate [122]. (The <0001>B direction in wurtzite structure is equivalent to the <111>B of zincblende polytype.) A complete and accurate description in the VLS case would involve catalyst chemical potential, solid–liquid interface energy for different possible crystal planes in contact with the liquid catalyst, solid-vapor surface energy of nanowire sides, liquid–vapor interface energy, edge energies of the top facet, edge energies of the growing island, [49] edge energies at nanowire side corners, if or not a new layer has well-defined low-index facets or is the surface rather rounded, [123] effect of liquid ordering, [45] etc. These individual terms are a function of the growth parameters and catalyst composition. As mentioned in the previous paragraph, most of these values have not been measured yet. But all these factors present, perhaps there is some key factor(s) which overpowers at typical growth conditions?

A very interesting but unresolved question is the diffusion pathway of the reactants. If the group V or group VI species is expected to hardly dissolve in the catalyst during compound nanowire growth, is it necessary that it should diffuse through the volume of the catalyst? Could these species be diffusing through the catalyst-nanowire surface instead? With the current technology it is not possible to watch the trajectory of each individual atom. However, perhaps there could be

some strategic in situ experiments, which in combination with appropriate rigorous theoretical simulations, can solve this puzzle. The radius dependence of the ledge-flow time might distinguish if the diffusion is through bulk or interface. The dynamics of the ledge-flow and the shape of the growing layer might also serve as a tool. That said, it is not necessary that there be a unique answer to this puzzle even for a given catalyst-nanowire system and catalyst phase (i.e. VLS or VSS), perhaps it could be dependent on the growth conditions. Another approach to this puzzle could be – diffusion need not even be the rate limiting process; in such a case why care about it. But this is nonetheless an interesting unanswered riddle, where in situ TEM can be extremely valuable.

10. Summary

Several in situ techniques, including in situ TEM, has been used to study nanowire growth. In situ TEM studies revealed that the growth dynamics of compound nanowires (e.g. III-V nanowires like GaAs) is fundamentally different from elemental nanowires. This can be understood by the difference in solubility of the nanowire species in the catalyst, which was also investigated by in situ TEM. Due to this concentration difference the layer nucleation and layer completion processes could be independently controlled. The growth dynamics has been studied in relation with the crystal structure and nanowire-catalyst interface morphology.

Author details

Carina B. Maliakkal
Centre for Analysis and Synthesis, Lund University, Lund, Sweden

*Address all correspondence to: carina_babu.maliakkal@chem.lu.se, carinab.maliakkal@gmail.com

References

[1] Glas F, Harmand J-C, Patriarche G. Why Does Wurtzite Form in Nanowires of III-V Zinc Blende Semiconductors? Phys Rev Lett. 2007 Oct 5;99(14):146101.

[2] Persson AI, Larsson MW, Stenström S, Ohlsson BJ, Samuelson L, Wallenberg LR. Solid-phase diffusion mechanism for GaAs nanowire growth. Nature Materials. 2004 Oct;3(10):677-681.

[3] Joyce HJ, Wong-Leung J, Gao Q, Tan HH, Jagadish C. Phase Perfection in Zinc Blende and Wurtzite III–V Nanowires Using Basic Growth Parameters. Nano Lett. 2010 Mar 10;10(3):908-915.

[4] Dick KA, Caroff P, Bolinsson J, Messing ME, Johansson J, Deppert K, et al. Control of III–V nanowire crystal structure by growth parameter tuning. Semicond Sci Technol. 2010;25(2):024009.

[5] Hu J, Ouyang M, Yang P, Lieber CM. Controlled growth and electrical properties of heterojunctions of carbon nanotubes and silicon nanowires. Nature. 1999 May;399(6731):48-51.

[6] Guo YN, Zou J, Paladugu M, Wang H, Gao Q, Tan HH, et al. Structural characteristics of GaSb/GaAs nanowire heterostructures grown by metal-organic chemical vapor deposition. Appl Phys Lett. 2006 Dec 4;89(23):231917.

[7] Caroff P, Messing ME, Borg BM, Dick KA, Deppert K, Wernersson L-E. InSb heterostructure nanowires: MOVPE growth under extreme lattice mismatch. Nanotechnology. 2009 Nov;20(49):495606.

[8] Barth S, S. Seifner M, Bernardi J. Microwave-assisted solution–liquid–solid growth of Ge 1–x Sn x nanowires with high tin content. Chemical Communications. 2015;51(61):12282-12285.

[9] Güniat L, Caroff P, Fontcuberta i Morral A. Vapor Phase Growth of Semiconductor Nanowires: Key Developments and Open Questions. Chem Rev. 2019 Aug 14;119(15):8958-8971.

[10] Hsueh T-J, Hsu C-L, Chang S-J, Guo P-W, Hsieh J-H, Chen I-C. Cu2O/n-ZnO nanowire solar cells on ZnO:Ga/glass templates. Scripta Materialia. 2007 Jul 1;57(1):53-56.

[11] Krogstrup P, Jørgensen HI, Heiss M, Demichel O, Holm JV, Aagesen M, et al. Single-nanowire solar cells beyond the Shockley–Queisser limit. Nature Photonics. 2013 Apr;7(4):306-310.

[12] Wallentin J, Anttu N, Asoli D, Huffman M, Åberg I, Magnusson MH, et al. InP Nanowire Array Solar Cells Achieving 13.8% Efficiency by Exceeding the Ray Optics Limit. Science. 2013 Mar 1;339(6123):1057-1060.

[13] Otnes G, Borgström MT. Towards high efficiency nanowire solar cells. Nano Today. 2017 Feb 1;12:31-45.

[14] Cui Y, Duan X, Hu J, Lieber CM. Doping and Electrical Transport in Silicon Nanowires. J Phys Chem B. 2000 Jun 1;104(22):5213-5216.

[15] Huang Y, Duan X, Cui Y, Lauhon LJ, Kim K-H, Lieber CM. Logic Gates and Computation from Assembled Nanowire Building Blocks. Science. 2001 Nov 9;294(5545):1313-1317.

[16] Li Y, Qian F, Xiang J, Lieber CM. Nanowire electronic and optoelectronic devices. Materials Today. 2006 Oct 1;9(10):18-27.

[17] Könenkamp R, Word RC, Schlegel C. Vertical nanowire light-emitting diode. Appl Phys Lett. 2004 Dec 9;85(24):6004-6006.

[18] Johnson JC, Choi H-J, Knutsen KP, Schaller RD, Yang P, Saykally RJ. Single gallium nitride nanowire lasers. Nature Materials. 2002 Oct;1(2):106-110.

[19] Huang MH, Mao S, Feick H, Yan H, Wu Y, Kind H, et al. Room-Temperature Ultraviolet Nanowire Nanolasers. Science. 2001 Jun 8;292(5523):1897-1899.

[20] Wang J, Gudiksen MS, Duan X, Cui Y, Lieber CM. Highly Polarized Photoluminescence and Photodetection from Single Indium Phosphide Nanowires. Science. 2001 Aug 24;293(5534):1455-1457.

[21] Yan C, Wang J, Wang X, Kang W, Cui M, Foo CY, et al. An Intrinsically Stretchable Nanowire Photodetector with a Fully Embedded Structure. Advanced Materials. 2014;26(6):943-950.

[22] Hochbaum AI, Chen R, Delgado RD, Liang W, Garnett EC, Najarian M, et al. Enhanced thermoelectric performance of rough silicon nanowires. Nature. 2008 Jan;451(7175):163-167.

[23] Wei Q, Lieber CM. Synthesis of Single Crystal Bismuth-Telluride and Lead-Telluride Nanowires for New Thermoelectric Materials. MRS Online Proceedings Library Archive. 1999 ed;581.

[24] Cui Y, Wei Q, Park H, Lieber CM. Nanowire Nanosensors for Highly Sensitive and Selective Detection of Biological and Chemical Species. Science. 2001 Aug 17;293(5533):1289-1292.

[25] Zhao Y, You SS, Zhang A, Lee J-H, Huang J, Lieber CM. Scalable ultrasmall three-dimensional nanowire transistor probes for intracellular recording. Nature Nanotechnology. 2019 Aug;14(8):783-790.

[26] Hazard TM, Gyenis A, Di Paolo A, Asfaw AT, Lyon SA, Blais A, et al. Nanowire Superinductance Fluxonium Qubit. Phys Rev Lett. 2019 Jan 10;122(1):010504.

[27] Ku J, Manucharyan V, Bezryadin A. Superconducting nanowires as nonlinear inductive elements for qubits. Phys Rev B. 2010 Oct 13;82(13):134518.

[28] Ek M, Filler MA. Atomic-Scale Choreography of Vapor–Liquid–Solid Nanowire Growth. Acc Chem Res. 2018 Jan 16;51(1):118-126.

[29] Tian B, Xie P, Kempa TJ, Bell DC, Lieber CM. Single-crystalline kinked semiconductor nanowire superstructures. Nature Nanotechnology. 2009 Dec;4(12):824-829.

[30] Hayden O, Agarwal R, Lu W. Semiconductor nanowire devices. Nano Today. 2008 Oct 1;3(5):12-22.

[31] Riveros G, Gómez H, Schrebler R, Marotti RE, Dalchiele EA. An In Situ EIS Study during the Electrochemical Growth of Copper Nanowires into Porous Polycarbonate Membranes. Electrochem Solid-State Lett. 2007 Dec 27;11(3):K19.

[32] Khan MI, Penchev M, Jing X, Wang X, Bozhilov KN, Ozkan M, et al. Electrochemical Growth of InSb Nanowires and Report of a Single Nanowire Field Effect Transistor. Journal of Nanoelectronics and Optoelectronics. 2008 Jul 1;3(2):199-202.

[33] Fahrenkrug E, Gu J, Jeon S, Veneman PA, Goldman RS, Maldonado S. Room-Temperature Epitaxial Electrodeposition of Single-Crystalline Germanium Nanowires

at the Wafer Scale from an Aqueous Solution. Nano Lett. 2014 Feb 12;14(2):847-852.

[34] Cheek Q, Fahrenkrug E, Hlynchuk S, Alsem DH, Salmon NJ, Maldonado S. In Situ Transmission Electron Microscopy Measurements of Ge Nanowire Synthesis with Liquid Metal Nanodroplets in Water. ACS Nano. 2020 Mar 24;14(3):2869-2879.

[35] Wagner RS, Ellis WC. Vapor-liquid-solid mechanism of single crystal growth. Appl Phys Lett. 1964 Mar 1;4(5):89-90.

[36] Bootsma GA, Gassen HJ. A quantitative study on the growth of silicon whiskers from silane and germanium whiskers from germane. Journal of Crystal Growth. 1971 Aug 1;10(3):223-234.

[37] Schouler MC, Cheynet MC, Sestier K, Garden J, Gadelle P. New filamentous deposits in the boron-carbon system. Carbon. 1997 Jan 1;35(7):993-1000.

[38] Mandl B, Stangl J, Hilner E, Zakharov AA, Hillerich K, Dey AW, et al. Growth Mechanism of Self-Catalyzed Group III–V Nanowires. Nano Lett. 2010 Nov 10;10(11):4443-4449.

[39] Ramdani MR, Harmand JC, Glas F, Patriarche G, Travers L. Arsenic Pathways in Self-Catalyzed Growth of GaAs Nanowires. Crystal Growth & Design. 2013 Jan 2;13(1):91-96.

[40] Heon Kim Y, Woo Park D, Jun Lee S. Gallium-droplet behaviors of self-catalyzed GaAs nanowires: A transmission electron microscopy study. Appl Phys Lett. 2012 Jan 16;100(3):033117.

[41] Zhang Z, Wang Y, Li H, Yuan W, Zhang X, Sun C, et al. Atomic-Scale Observation of Vapor–Solid Nanowire Growth via Oscillatory Mass Transport. ACS Nano. 2016 Jan 26;10(1):763-769.

[42] Lee SC, Dawson LR, Brueck SRJ, Jiang Y-B. Anisotropy of selective epitaxy in nanoscale-patterned growth: GaAs nanowires selectively grown on a SiO2-patterned (001) substrate by molecular-beam epitaxy. Journal of Applied Physics. 2005 Dec 1;98(11):114312.

[43] Noborisaka J, Motohisa J, Hara S, Fukui T. Fabrication and characterization of freestanding GaAs/AlGaAs core-shell nanowires and AlGaAs nanotubes by using selective-area metalorganic vapor phase epitaxy. Appl Phys Lett. 2005 Aug 24;87(9):093109.

[44] Jacobsson D, Lehmann S, Dick KA. Zincblende-to-wurtzite interface improvement by group III loading in Au-seeded GaAs nanowires. Phys Status Solidi RRL. 2013 Oct 1;7(10):855-859.

[45] Oh SH, Chisholm MF, Kauffmann Y, Kaplan WD, Luo W, Rühle M, et al. Oscillatory Mass Transport in Vapor-Liquid-Solid Growth of Sapphire Nanowires. Science. 2010 Oct 22;330(6003):489-493.

[46] Wen C-Y, Tersoff J, Hillerich K, Reuter MC, Park JH, Kodambaka S, et al. Periodically Changing Morphology of the Growth Interface in Si, Ge, and GaP Nanowires. Phys Rev Lett. 2011 Jul 6;107(2):025503.

[47] Gamalski AD, Ducati C, Hofmann S. Cyclic Supersaturation and Triple Phase Boundary Dynamics in Germanium Nanowire Growth. J Phys Chem C. 2011 Mar 24;115(11):4413-4417.

[48] Tornberg M, Maliakkal CB, Jacobsson D, Dick KA, Johansson J. Limits of III–V Nanowire Growth Based on Droplet Dynamics. J Phys Chem Lett. 2020 Apr 16;11(8):2949-2954.

[49] Harmand J-C, Patriarche G, Glas F, Panciera F, Florea I, Maurice J-L, et al. Atomic Step Flow on a Nanofacet. Phys Rev Lett. 2018 Oct 19;121(16):166101.

[50] Tchernycheva M, Harmand JC, Patriarche G, Travers L, Cirlin GE. Temperature conditions for GaAs nanowire formation by Au-assisted molecular beam epitaxy. Nanotechnology. 2006 Jul;17(16):4025-4030.

[51] Jo J, Tchoe Y, Yi G-C, Kim M. Real-Time Characterization Using in situ RHEED Transmission Mode and TEM for Investigation of the Growth Behaviour of Nanomaterials. Scientific Reports. 2018 Jan 26;8(1):1694.

[52] Heurlin M, Anttu N, Camus C, Samuelson L, Borgström MT. In Situ Characterization of Nanowire Dimensions and Growth Dynamics by Optical Reflectance. Nano Lett. 2015 May 13;15(5):3597-3602.

[53] Braun MR, Güniat L, Morral AFI, McIntyre PC. In-situ reflectometry to monitor locally-catalyzed initiation and growth of nanowire assemblies. Nanotechnology. 2020 Jun;31(33):335703.

[54] Schroth P, Köhl M, Hornung J-W, Dimakis E, Somaschini C, Geelhaar L, et al. Evolution of Polytypism in GaAs Nanowires during Growth Revealed by Time-Resolved in situ x-ray Diffraction. Phys Rev Lett. 2015 Feb 5;114(5):055504.

[55] Krogstrup P, Hannibal Madsen M, Hu W, Kozu M, Nakata Y, Nygård J, et al. In-situ x-ray characterization of wurtzite formation in GaAs nanowires. Appl Phys Lett. 2012 Feb 27;100(9):093103.

[56] Kirkham M, Wang ZL, Snyder RL. Tracking the catalyzed growth process of nanowires by in situ x-ray diffraction. Journal of Applied Physics. 2010 Jul 1;108(1):014304.

[57] Sivaram SV, Hui HY, de la Mata M, Arbiol J, Filler MA. Surface Hydrogen Enables Subeutectic Vapor–Liquid–Solid Semiconductor Nanowire Growth. Nano Lett. 2016 Nov 9;16(11):6717-6723.

[58] Sivaram SV, Shin N, Chou L-W, Filler MA. Direct Observation of Transient Surface Species during Ge Nanowire Growth and Their Influence on Growth Stability. J Am Chem Soc. 2015 Aug 12;137(31):9861-9869.

[59] Shin N, Chi M, Filler MA. Interplay between Defect Propagation and Surface Hydrogen in Silicon Nanowire Kinking Superstructures. ACS Nano. 2014 Apr 22;8(4):3829-3835.

[60] Shin N, Filler MA. Controlling Silicon Nanowire Growth Direction via Surface Chemistry. Nano Lett. 2012 Jun 13;12(6):2865-2870.

[61] Fernández-Garrido S, Zettler JK, Geelhaar L, Brandt O. Monitoring the Formation of Nanowires by Line-of-Sight Quadrupole Mass Spectrometry: A Comprehensive Description of the Temporal Evolution of GaN Nanowire Ensembles. Nano Lett. 2015 Mar 11;15(3):1930-1937.

[62] Volkov Y, Mitchell S, Gaponik N, Rakovich YP, Donegan JF, Kelleher D, et al. In-Situ Observation of Nanowire Growth from Luminescent CdTe Nanocrystals in a Phosphate Buffer Solution. ChemPhysChem. 2004 Oct 18;5(10):1600-1602.

[63] Kolíbal M, Pejchal T, Vystavěl T, Šikola T. The Synergic Effect of Atomic Hydrogen Adsorption and Catalyst Spreading on Ge Nanowire Growth Orientation and Kinking. Nano Lett. 2016 Aug 10;16(8):4880-4886.

[64] Prikhodko SV, Sitzman S, Gambin V, Kodambaka S. In situ

electron backscattered diffraction of individual GaAs nanowires. Ultramicroscopy. 2008 Dec 1;109(1):133-138.

[65] Kolíbal M, Vystavěl T, Varga P, Šikola T. Real-Time Observation of Collector Droplet Oscillations during Growth of Straight Nanowires. Nano Lett. 2014 Apr 9;14(4):1756-1761.

[66] Sun Y, Gao J, Zhu R, Xu J, Chen L, Zhang J, et al. In situ observation of ZnO nanowire growth on zinc film in environmental scanning electron microscope. J Chem Phys. 2010 Mar 28;132(12):124705.

[67] Huang X, Wang Z-J, Weinberg G, Meng X-M, Willinger M-G. In Situ Scanning Electron Microscopy Observation of Growth Kinetics and Catalyst Splitting in Vapor–Liquid–Solid Growth of Nanowires. Advanced Functional Materials. 2015 Oct 1;25(37):5979-5987.

[68] Wu Y, Yang P. Direct Observation of Vapor−Liquid−Solid Nanowire Growth. J Am Chem Soc. 2001 Apr 1;123(13):3165-3166.

[69] Ross FM, Tersoff J, Reuter MC. Sawtooth Faceting in Silicon Nanowires. Phys Rev Lett. 2005 Sep 29;95(14):146104.

[70] Kodambaka S, Tersoff J, Reuter MC, Ross FM. Diameter-Independent Kinetics in the Vapor-Liquid-Solid Growth of Si Nanowires. Phys Rev Lett. 2006 Mar 9;96(9):096105.

[71] Hannon JB, Kodambaka S, Ross FM, Tromp RM. The influence of the surface migration of gold on the growth of silicon nanowires. Nature. 2006 Mar;440(7080):69-71.

[72] Kodambaka S, Tersoff J, Reuter MC, Ross FM. Germanium Nanowire Growth Below the Eutectic Temperature. Science. 2007 May 4;316(5825):729-732.

[73] Hofmann S, Sharma R, Wirth CT, Cervantes-Sodi F, Ducati C, Kasama T, et al. Ledge-flow-controlled catalyst interface dynamics during Si nanowire growth. Nature Materials. 2008 May;7(5):372-375.

[74] Wen C-Y, Reuter MC, Bruley J, Tersoff J, Kodambaka S, Stach EA, et al. Formation of Compositionally Abrupt Axial Heterojunctions in Silicon-Germanium Nanowires. Science. 2009 Nov 27;326(5957):1247-1250.

[75] Madras P, Dailey E, Drucker J. Kinetically Induced Kinking of Vapor−Liquid−Solid Grown Epitaxial Si Nanowires. Nano Lett. 2009 Nov 11;9(11):3826-3830.

[76] Kallesøe C, Wen C-Y, Mølhave K, Bøggild P, Ross FM. Measurement of Local Si-Nanowire Growth Kinetics Using In situ Transmission Electron Microscopy of Heated Cantilevers. Small. 2010 Sep 20;6(18):2058-2064.

[77] Wen C-Y, Reuter MC, Tersoff J, Stach EA, Ross FM. Structure, Growth Kinetics, and Ledge Flow during Vapor−Solid−Solid Growth of Copper-Catalyzed Silicon Nanowires. Nano Lett. 2010 Feb 10;10(2):514-519.

[78] Wen C-Y, Tersoff J, Reuter MC, Stach EA, Ross FM. Step-Flow Kinetics in Nanowire Growth. Phys Rev Lett. 2010 Nov 5;105(19):195502.

[79] Diaz RE, Sharma R, Jarvis K, Zhang Q, Mahajan S. Direct observation of nucleation and early stages of growth of GaN nanowires. Journal of Crystal Growth. 2012 Feb 15;341(1):1-6.

[80] Chou Y-C, Hillerich K, Tersoff J, Reuter MC, Dick KA, Ross FM. Atomic-Scale Variability and Control of III-V Nanowire Growth Kinetics. Science. 2014 Jan 17;343(6168):281-284.

[81] Schwarz KW, Tersoff J, Kodambaka S, Ross FM.

Jumping-Catalyst Dynamics in Nanowire Growth. Phys Rev Lett. 2014 Jul 30;113(5):055501.

[82] Chou Y-C, Panciera F, C. Reuter M, A. Stach E, M. Ross F. Nanowire growth kinetics in aberration corrected environmental transmission electron microscopy. Chemical Communications. 2016;52(33):5686-5689.

[83] Gamalski AD, Tersoff J, Stach EA. Atomic Resolution in Situ Imaging of a Double-Bilayer Multistep Growth Mode in Gallium Nitride Nanowires. Nano Lett. 2016 Apr 13;16(4):2283-2288.

[84] Jacobsson D, Panciera F, Tersoff J, Reuter MC, Lehmann S, Hofmann S, et al. Interface dynamics and crystal phase switching in GaAs nanowires. Nature. 2016 Mar 16;531(7594):317.

[85] Panciera F, Norton MM, Alam SB, Hofmann S, Mølhave K, Ross FM. Controlling nanowire growth through electric field-induced deformation of the catalyst droplet. Nature Communications. 2016 Jul 29;7:12271.

[86] Panciera F, Tersoff J, Gamalski AD, Reuter MC, Zakharov D, Stach EA, et al. Surface Crystallization of Liquid Au–Si and Its Impact on Catalysis. Advanced Materials. 2019;31(5):1806544.

[87] Kim BJ, Tersoff J, Kodambaka S, Reuter MC, Stach EA, Ross FM. Kinetics of Individual Nucleation Events Observed in Nanoscale Vapor-Liquid-Solid Growth. Science. 2008 Nov 14;322(5904):1070-1073.

[88] Kim BJ, Wen C-Y, Tersoff J, Reuter MC, Stach EA, Ross FM. Growth Pathways in Ultralow Temperature Ge Nucleation from Au. Nano Lett. 2012 Nov 14;12(11):5867-5872.

[89] Maliakkal CB, Jacobsson D, Tornberg M, Persson AR, Johansson J, Wallenberg R, et al. In situ analysis of catalyst composition during gold catalyzed GaAs nanowire growth. Nat Commun. 2019 Oct 8;10(1):1-9.

[90] Maliakkal CB, Mårtensson EK, Tornberg MU, Jacobsson D, Persson AR, Johansson J, et al. Independent Control of Nucleation and Layer Growth in Nanowires. ACS Nano. 2020 Feb 12;14(4):3868-3875.

[91] Lenrick F, Ek M, Deppert K, Samuelson L, Wallenberg LR. Straight and kinked InAs nanowire growth observed in situ by transmission electron microscopy. Nano Res. 2014 Aug 1;7(8):1188-1194.

[92] Song M, Lee J, Wang B, A. Legg B, Hu S, Chun J, et al. In situ characterization of kinetics and mass transport of PbSe nanowire growth via LS and VLS mechanisms. Nanoscale. 2019;11(13):5874-5878.

[93] Mølhave K, Wacaser BA, Petersen DH, Wagner JB, Samuelson L, Bøggild P. Epitaxial Integration of Nanowires in Microsystems by Local Micrometer-Scale Vapor-Phase Epitaxy. Small. 2008;4(10):1741-1746.

[94] Kodambaka S, Hannon JB, Tromp RM, Ross FM. Control of Si Nanowire Growth by Oxygen. Nano Lett. 2006 Jun 1;6(6):1292-1296.

[95] Glas F, Harmand J-C, Patriarche G. Nucleation Antibunching in Catalyst-Assisted Nanowire Growth. Phys Rev Lett. 2010 Mar 31;104(13):135501.

[96] Dubrovskii VG, Sibirev NV, Harmand JC, Glas F. Growth kinetics and crystal structure of semiconductor nanowires. Phys Rev B. 2008 Dec 1;78(23):235301.

[97] Dubrovskii VG, Sokolova ZhV, Rylkova MV, Zhiglinsky AA. Composition and contact angle of Au-III-V droplets on top of Au-catalyzed III-V nanowires. Materials Physics & Mechanics. 2018 Mar;36(1):1-7.

[98] Dubrovskii VG, Sibirev NV. Growth rate of a crystal facet of arbitrary size and growth kinetics of vertical nanowires. Phys Rev E. 2004 Sep 15;70(3):031604.

[99] Panciera F, Baraissov Z, Patriarche G, Dubrovskii VG, Glas F, Travers L, et al. Phase Selection in Self-catalyzed GaAs Nanowires. Nano Lett. 2020 Mar 11;20(3):1669-1675.

[100] Stach EA, Pauzauskie PJ, Kuykendall T, Goldberger J, He R, Yang P. Watching GaN Nanowires Grow. Nano Lett. 2003 Jun 1;3(6):867-869.

[101] Massalski TB. Binary alloy phase diagrams. II. Materials Park, Ohio: American Society for Metals; 1990.

[102] Glas F, Ramdani MR, Patriarche G, Harmand J-C. Predictive modeling of self-catalyzed III-V nanowire growth. Phys Rev B. 2013 Nov 8;88(19):195304.

[103] Mårtensson EK, Lehmann S, Dick KA, Johansson J. Simulation of GaAs Nanowire Growth and Crystal Structure. Nano Lett. 2019 Feb 13;19(2):1197-1203.

[104] Dubrovskii VG. Influence of the group V element on the chemical potential and crystal structure of Au-catalyzed III-V nanowires. Appl Phys Lett. 2014 Feb 3;104(5):053110.

[105] Dubrovskii VG, Grecenkov J. Zeldovich Nucleation Rate, Self-Consistency Renormalization, and Crystal Phase of Au-Catalyzed GaAs Nanowires. Crystal Growth & Design. 2015 Jan 7;15(1):340-347.

[106] D. Leshchenko E, Ghasemi M, G. Dubrovskii V, Johansson J. Nucleation-limited composition of ternary III–V nanowires forming from quaternary gold based liquid alloys. CrystEngComm. 2018;20(12):1649-1655.

[107] Harmand JC, Patriarche G, Péré-Laperne N, Mérat-Combes M-N, Travers L, Glas F. Analysis of vapor-liquid-solid mechanism in Au-assisted GaAs nanowire growth. Appl Phys Lett. 2005 Nov 7;87(20):203101.

[108] Tornberg M, Jacobsson D, Persson AR, Wallenberg R, Dick KA, Kodambaka S. Kinetics of Au–Ga Droplet Mediated Decomposition of GaAs Nanowires. Nano Lett. 2019 Jun 12;19(6):3498-3504.

[109] Prince A, Raynor GV, Evans DS, Institute of Metals. Phase diagrams of ternary gold alloys. London; Brookfield, VT: Institute of Metals; 1990.

[110] Lehmann S, Jacobsson D, Dick KA. Crystal phase control in GaAs nanowires: opposing trends in the Ga- and As-limited growth regimes. Nanotechnology. 2015;26(30):301001.

[111] Gagliano L, Belabbes A, Albani M, Assali S, Verheijen MA, Miglio L, et al. Pseudodirect to Direct Compositional Crossover in Wurtzite GaP/InxGa1–xP Core–Shell Nanowires. Nano Lett. 2016 Dec 14;16(12):7930-7936.

[112] Assali S, Greil J, Zardo I, Belabbes A, de Moor MWA, Koelling S, et al. Optical study of the band structure of wurtzite GaP nanowires. Journal of Applied Physics. 2016 Jul 25;120(4):044304.

[113] Maliakkal CB, Gokhale M, Parmar J, Bapat RD, Chalke BA, Ghosh S, et al. Growth, structural and optical characterization of wurtzite GaP nanowires. Nanotechnology. 2019 Apr;30(25):254002.

[114] Dick KA, Thelander C, Samuelson L, Caroff P. Crystal Phase Engineering in Single InAs Nanowires. Nano Lett. 2010 Sep 8;10(9):3494-3499.

[115] Akopian N, Patriarche G, Liu L, Harmand J-C, Zwiller V. Crystal Phase

Quantum Dots. Nano Lett. 2010 Apr 14;10(4):1198-1201.

[116] Akiyama T, Sano K, Nakamura K, Ito T. An Empirical Potential Approach to Wurtzite–Zinc-Blende Polytypism in Group III–V Semiconductor Nanowires. Jpn J Appl Phys. 2006 Feb 24;45(3L):L275.

[117] Pankoke V, Kratzer P, Sakong S. Calculation of the diameter-dependent polytypism in GaAs nanowires from an atomic motif expansion of the formation energy. Phys Rev B. 2011 Aug 10;84(7):075455.

[118] Johansson J, Bolinsson J, Ek M, Caroff P, Dick KA. Combinatorial Approaches to Understanding Polytypism in III–V Nanowires. ACS Nano. 2012 Jul 24;6(7):6142-6149.

[119] Moll N, Kley A, Pehlke E, Scheffler M. GaAs equilibrium crystal shape from first principles. Phys Rev B. 1996 Sep 15;54(12):8844-8855.

[120] Messmer C, Bilello JC. The surface energy of Si, GaAs, and GaP. Journal of Applied Physics. 1981 Jul 1;52(7):4623-4629.

[121] Hui TA, Wang F, Han N, Yip S, Xiu F, J. Hou J, et al. High-performance indium phosphide nanowires synthesized on amorphous substrates: from formation mechanism to optical and electrical transport measurements. Journal of Materials Chemistry. 2012;22(21):10704-10708.

[122] Heurlin M, Magnusson MH, Lindgren D, Ek M, Wallenberg LR, Deppert K, et al. Continuous gas-phase synthesis of nanowires with tunable properties. Nature. 2012 Dec;492(7427):90-94.

[123] Jiang N, Wong-Leung J, Joyce HJ, Gao Q, Tan HH, Jagadish C. Understanding the True Shape of Au-Catalyzed GaAs Nanowires. Nano Lett. 2014 Oct 8;14(10):5865-5872.